IOP Publishing J. Neural Eng. 20 (2023) 016016 https://doi.org/10.1088/1741-2552/acabe8

Journal of Neural Engineering

OPEN ACCESS

RECEIVED
14 September 2022

REVISED
18 November 2022

ACCEPTED FOR PUBLICATION
15 December 2022

PUBLISHED
18 January 2023

PAPER

Using a high-frequency carrier does not improve comfort of transcutaneous spinal cord stimulation

Ashley N Dalrymple[1,2,*], **Charli Ann Hooper**[1,2,3], **Minna G Kuriakose**[4,6], **Marco Capogrosso**[4,5,6,7] and **Douglas J Weber**[1,2,8,*]

[1] Department of Mechanical Engineering, Carnegie Mellon University, Pittsburgh, PA, United States of America
[2] NeuroMechatronics Lab, Carnegie Mellon University, Pittsburgh, PA, United States of America
[3] Department of Biomedical Engineering, Carnegie Mellon University, Pittsburgh, PA, United States of America
[4] Department of Bioengineering, University of Pittsburgh, Pittsburgh, PA, United States of America
[5] Department of Neurological Surgery, University of Pittsburgh, Pittsburgh, PA, United States of America
[6] Rehab Neural Engineering Labs, University of Pittsburgh, Pittsburgh, PA, United States of America
[7] Center for Neural Basis of Cognition, Pittsburgh, PA, United States of America
[8] Neuroscience Institute, Carnegie Mellon University, Pittsburgh, PA, United States of America
[*] Authors to whom any correspondence should be addressed.

E-mail: adalrymple@cmu.edu and dougweber@cmu.edu

Keywords: transcutaneous spinal cord stimulation, high-frequency carrier, neuromodulation, reflexes, pain tolerance

Supplementary material for this article is available online

Abstract

Objective. Spinal cord neuromodulation has gained much attention for demonstrating improved motor recovery in people with spinal cord injury, motivating the development of clinically applicable technologies. Among them, transcutaneous spinal cord stimulation (tSCS) is attractive because of its non-invasive profile. Many tSCS studies employ a high-frequency (10 kHz) carrier, which has been reported to reduce stimulation discomfort. However, these claims have come under scrutiny in recent years. The purpose of this study was to determine whether using a high-frequency carrier for tSCS is more comfortable at therapeutic amplitudes, which evoke posterior root-muscle (PRM) reflexes. *Approach.* In 16 neurologically intact participants, tSCS was delivered using a 1 ms long monophasic pulse with and without a high-frequency carrier. Stimulation amplitude and pulse duration were varied and PRM reflexes were recorded from the soleus, gastrocnemius, and tibialis anterior muscles. Participants rated their discomfort during stimulation from 0 to 10 at PRM reflex threshold. *Main Results.* At PRM reflex threshold, the addition of a high-frequency carrier (0.87 ± 0.2) was equally comfortable as conventional stimulation (1.03 ± 0.18) but required approximately double the charge to evoke the PRM reflex (conventional: 32.4 ± 9.2 μC; high-frequency carrier: 62.5 ± 11.1 μC). Strength-duration curves for tSCS with a high-frequency carrier had a rheobase that was 4.8× greater and a chronaxie that was 5.7× narrower than the conventional monophasic pulse, indicating that the addition of a high-frequency carrier makes stimulation less efficient in recruiting neural activity in spinal roots. *Significance.* Using a high-frequency carrier for tSCS is equally as comfortable and less efficient as conventional stimulation at amplitudes required to stimulate spinal dorsal roots.

1. Introduction

Neuromodulation of the spinal cord can be used to treat chronic pain (Shealy *et al* 1967, Caylor *et al* 2019) and improve motor function after stroke (Powell *et al* 2022) and spinal cord injury (Carhart *et al* 2004, Harkema *et al* 2011, Angeli *et al* 2018, Gill *et al* 2018, Rowald *et al* 2022). Transcutaneous spinal cord stimulation (tSCS) is a non-invasive neuromodulation technique that uses adhesive electrodes on or adjacent to the spine to activate primary afferent neurons in the spinal roots, particularly the large diameter afferent fibers, similar to epidural spinal cord stimulation (eSCS) (Capogrosso *et al* 2013, Hofstoetter

et al 2018). tSCS has the potential to be a more accessible neuromodulation therapy that could reach people without access to surgical procedures or those who are contra-indicated or unwilling to receive an eSCS implant. To date, tSCS has been demonstrated as an effective method to improve motor function in the arm and hand (Freyvert *et al* 2018, Gad *et al* 2018, Inanici *et al* 2018, 2021), trunk (Rath *et al* 2018, Sayenko *et al* 2019, Keller *et al* 2021), and legs (Hofstoetter *et al* 2013, 2015b, 2021, Gad *et al* 2017, 2019, Samejima *et al* 2022) in people with various neurological conditions.

tSCS (and eSCS) excite the large-diameter afferents in the spinal roots (Hofstoetter *et al* 2018, 2019), engaging spinal reflex pathways that facilitate activity in motoneurons. The evoked response can be recorded using electromyography (EMG) and is known as the posterior root-muscle (PRM) reflex (Minassian *et al* 2007). The PRM reflex is equivalent to the Hoffman (H)-reflex but engages multiple segments of spinal roots (Minassian *et al* 2007, Krenn *et al* 2013). Compared to eSCS with implanted electrodes, the current amplitudes required for tSCS are much higher. Since tSCS is delivered through electrodes placed on the skin, stimulation also activates cutaneous afferents and induces strong contractions in paraspinal muscles, both of which can cause discomfort.

The conventional waveform used for tSCS is a square pulse with a duration of 1–2 ms applied at 30–50 Hz to facilitate muscle activation (Hofstoetter *et al* 2014, 2015b, 2020, 2021, Gad *et al* 2017, Freyvert *et al* 2018, Knikou and Murray 2019). An alternative approach uses a high frequency carrier wave, typically 10 kHz, within the 1–2 ms pulse (Gerasimenko *et al* 2015a, 2015b, 2016, Gad *et al* 2018, 2019, Inanici *et al* 2018, 2021, Rath *et al* 2018, Sayenko *et al* 2019, Keller *et al* 2021). The concept of using a high-frequency carrier originates from Russia in the 1970's and is colloquially termed 'Russian current' (Ward and Shkuratova 2002, Manson *et al* 2020). The benefit of the high-frequency carrier, originally selected to be 2.5 kHz, was that it made the stimulation less painful. A later study found the optimal frequency for motor activation and minimal pain to be 10 kHz (Ward and Robertson 1998). Several tSCS studies claim that stimulation at 10 kHz is painless due to blocking of superficial nociceptive afferents, enabling use of higher stimulation amplitudes, such as those needed to target the spinal roots (Gerasimenko *et al* 2015a, Gad *et al* 2017, Sayenko *et al* 2019, Manson *et al* 2020, Inanici *et al* 2021).

A recent study aimed to characterize the maximal tolerable stimulation amplitude when using a conventional biphasic stimulation waveform with and without a 5 kHz carrier frequency (Manson *et al* 2020). They found that when the maximum tolerable stimulation amplitude was normalized to the stimulation amplitude required to evoke a PRM reflex, there was no difference between the waveforms. It is important to note that tSCS for neuromodulation to facilitate motor functions requires stimulation amplitudes near the PRM reflex threshold to be effective. Therefore, characterizing the comfort of tSCS at the PRM reflex threshold is of paramount interest.

Here, we compared stimulation thresholds for evoking PRM reflexes using a conventional 1 ms-long monophasic pulse with and without a 10 kHz carrier frequency for tSCS. Participants were asked to report a discomfort rating for the stimulation applied at the reflex threshold. We also extensively characterized the recruitment properties of PRM reflexes using both waveforms, using both recruitment curves and charge-duration curves, which has not been reported to date. We hypothesized that stimulation with a high-frequency carrier would have a higher PRM reflex threshold, and that at threshold, the high-frequency carrier waveform would not be more comfortable than the conventional waveform. As hypothesized, PRM reflex thresholds were higher for the high-frequency carrier waveform, which was equally as comfortable as the conventional waveform at its PRM reflex threshold. These results suggest that for tSCS, a high-frequency carrier waveform offers no advantages for reducing discomfort compared to a conventional waveform. Moreover, the higher stimulation charge needed to evoke a response with the high-frequency carrier waveform requires the stimulator to produce much higher voltages, increasing the power budget and risk of injury.

2. Materials and methods

2.1. Participants

Sixteen neurologically intact individuals participated in this study (mean age ± standard deviation (SD): 29.5 ± 6.9 years; eight female; table 1). We measured the circumference of each participant's waist and hips.

We excluded individuals from this study if they were younger than 18 years of age, were pregnant, or had any of the following: implanted electronic devices, metallic implants in their torso and/or legs, a serious bone or blood disease or infection, heart disease such as arrhythmia, or a history of stroke, spinal cord injury or disease, or muscle or nerve impairments affecting the lower limbs. This study was approved by the Internal Review Board at Carnegie Mellon University (STUDY2020_00000452) and conducted in accordance with the Declaration of Helsinki. All participants signed a written informed consent form prior to their enrollment in the study. No participants had prior experience with tSCS.

2.2. Study protocol

2.2.1. EMG electrode placement

We prepared the skin of the left lower leg for recording using abrasive gel (Lemon Prep, Mavidon, USA), alcohol wipes (Braha Industries, USA) and

Table 1. Demographic information for research participants. All participants were neurologically intact. HFC = high-frequency carrier.

Participant ID	Sex	Age (years)	Height (cm)	Weight (lbs)	Waist (cm)	Hip (cm)	First waveform
TSP01	Male	49	180	195	102	104	Conventional
TSP02	Female	23	165	125	69	92	HFC
TSP03	Female	25	160	119	71.5	90	Conventional
TSP04	Female	26	160	108	69	80	Conventional
TSP05	Male	28	193	190	91	97	HFC
TSP06	Male	40	178	170	86.5	93	Conventional
TSP07	Male	24	180	139	76	92	HFC
TSP08	Female	23	168	135	69.5	88.5	Conventional
TSP09	Male	24	180	139	76	92	HFC
TSP10	Female	29	160	149	82.5	95.5	Conventional
TSP11	Male	33	167	187	94.5	101.5	Conventional
TSP12	Male	32	170	165	84.5	94	HFC
TSP13	Male	32	185	176	86.5	97	Conventional
TSP14	Female	26	172	153	84	101.5	HFC
TSP15	Female	27	170	127	73	94	HFC
TSP16	Female	31	168	166	82	109	HFC
Mean ± STD	8 Female	26.3 ± 2.8	165.4 ± 4.9	135.3 ± 19.4	75.1 ± 6.6	93.8 ± 8.7	
Mean ± STD	8 Male	32.8 ± 8.4	177.8 ± 8.8	169.3 ± 23.2	87.3 ± 8.7	95.6 ± 5.7	

conductive electrode gel (Signa Gel, Parker Laboratories BV, NL). All data were collected while the participant sat comfortably in a chair with both knees positioned at a 120° angle (figure 1). We placed bipolar EMG electrodes (2 square 7/8″ × 7/8″ Ag|AgCl foam electrodes; MVAP Medical Supplies, USA) approximately 1 cm apart on the soleus, lateral and medial gastrocnemius, and tibialis anterior muscles of the left leg. We secured a ground electrode (4 × 5 cm pregelled Ag|AgCl Natus electrode; MVAP Medical Supplies, USA) onto the left patella. EMG data were recorded using the SAGA64+ (TMSi, NL) at a sampling rate of 4000 Hz and streamed into MATLAB (MathWorks, USA) using custom software. Stimulation was delivered using a DS8R stimulator with a firmware update to allow frequencies up to 10 kHz (Digitimer, UK). The stimulator was triggered using a PCIe-6353 I/O Device (National Instruments, USA), a BNC 2090 A connector accessory (National Instruments, USA) and custom MATLAB code.

2.2.2. PRM reflex threshold

Participants were oblivious to the composition of the waveforms, and we pseudo randomized and balanced which one was delivered first. We placed a round adhesive electrode for tSCS (3.2 cm diameter; ValuTrode, Axelgaard Manufacturing Co. Ltd, USA) paravertebrally left of the T12-L1 spinous processes, and a large rectangular electrode (7.5 × 13 cm, ValuTrode, Axelgaard Manufacturing Co. Ltd, USA) on the left anterior superior iliac spine. tSCS electrodes were placed paravertebrally to specifically target unilateral spinal roots and corresponding sensorimotor pathways that innervate the distal leg muscles (Krenn *et al* 2013, Calvert *et al* 2019). We wrapped the torso (6″ Coban, 3 M, USA) and placed a small piece of foam (12 × 17 cm) between the electrode and the back of the chair to maintain firm pressure on the stimulation site. Throughout the manuscript, we will refer to the monophasic pulse as the 'conventional waveform', and the pulse with the 10 kHz carrier frequency as the 'high-frequency carrier waveform'. Each of the following procedures were repeated for both waveforms.

We found the stimulation threshold for evoking a PRM reflex in the soleus muscle, which was the lowest stimulation amplitude that evoked a reflex response. We then determined the maximum PRM reflex amplitude (referred to as PRM_{Max}), which was defined as the stimulation amplitude at which the reflex amplitude no longer increased when stimulation amplitude increased. In this study, we did not exceed a stimulation amplitude of 180 mA.

2.2.3. Recruitment curves and confirming reflexes

We stimulated at 15 amplitudes between 5 mA below the PRM reflex threshold and 5–10 mA above the maximum amplitude, in a random order. We delivered the stimuli 10 s apart and repeated each stimulation amplitude four times. To confirm that the evoked responses were reflexive, we tested for rate-dependent depression (RDD). We delivered a series of three pulses 10 s apart, and a series of three pulses 1 s apart, at a stimulation amplitude approximately equal to 1.1–1.3 times PRM reflex threshold to ensure that it was suprathreshold.

2.2.4. Varying pulse duration

The high-frequency carrier waveform was active for half the time as the conventional waveform since the 10 kHz pulse train had a 50% duty cycle. Therefore, we sought to determine the effect of overall pulse duration on the PRM reflex threshold. We chose the following pulse durations: 100, 200, 300, 400, 500, 800, 1000, 1250, 1500, 1750, and 2000 μs. We determined

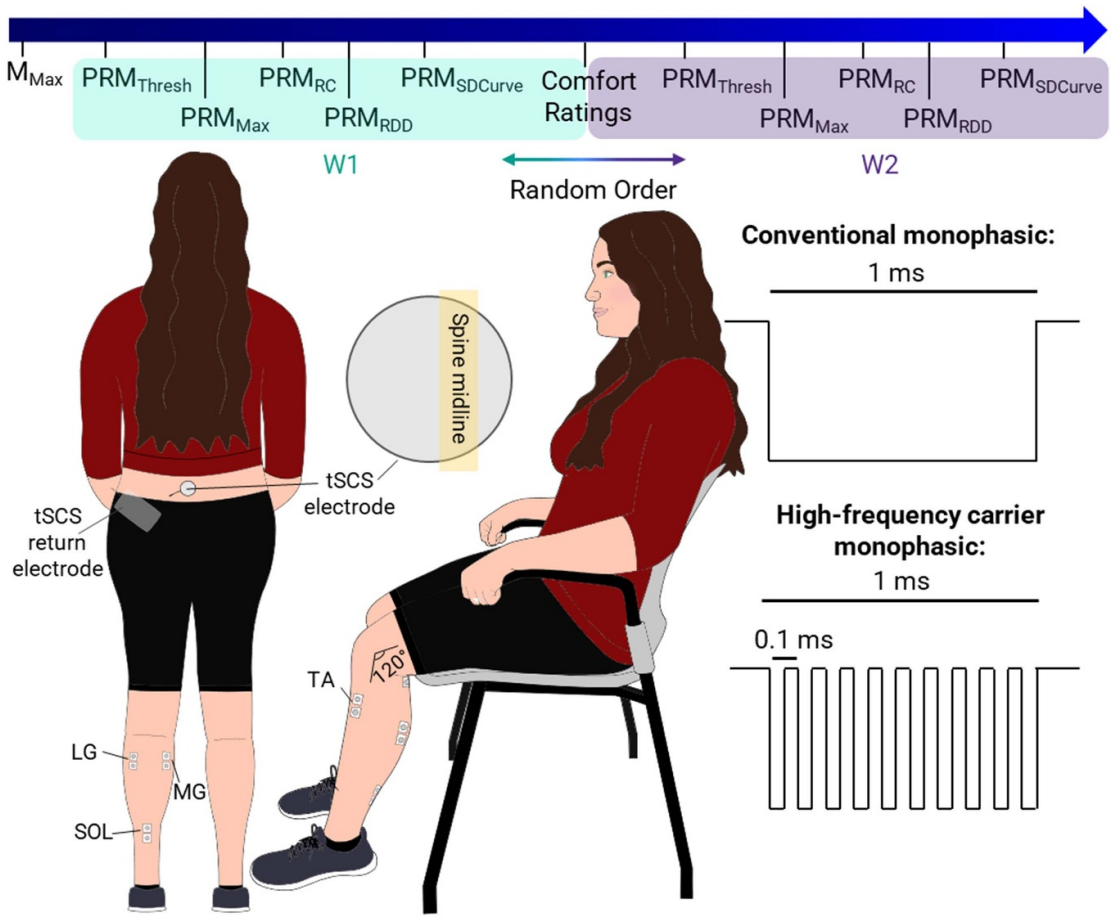

Figure 1. Experimental setup and procedures. The top bar shows the experimental timeline for collecting each measure. Waveform 1 (W1) and waveform 2 (W2) were either a conventional monophasic pulse or high-frequency carrier burst pulse, the order of which was pseudo-randomized across participants. The bottom left shows the experimental setup with electrode placements. Electromyography (EMG) electrodes were placed on the soleus (SOL), lateral gastrocnemius (LG), medial gastrocnemius (MG), and tibialis anterior (TA) muscles. Transcutaneous spinal cord stimulation (tSCS) was delivered using a round electrode placed lateral to the T12-L1 spinal levels. The tSCS return electrode was placed on the anterior superior iliac spine. The inset of the round electrode shows the location of the electrode relative to the midline of the spine. The bottom right shows the two different waveforms studied. M_{max} = motor maximum; PRM = posterior root muscle; Thresh = threshold; Max = maximum; RC = recruitment curve; RDD = rate-dependent depression, SDCurve = strength-duration curve.

PRM reflex threshold twice for each pulse duration and in a random order. It is important to note that for all other measures the pulse width was equal to 1 ms.

2.2.5. Discomfort scoring

We asked the participants to rate their discomfort from the electrical stimulation at the electrode site on a visual analog scale from 0 to 10, where 0 indicated no discomfort at all, and 10 indicated the most uncomfortable sensation imaginable. This was done at each threshold value across the various pulse durations. Moreover, we asked participants to rank the strength of the contraction of the paraspinal muscles on a scale of 0–10, where 0 was no contraction at all, and 10 was the strongest contraction imaginable. Paraspinal contractions were rated across stimulation amplitudes delivered between 20 and 80 mA, at 15 mA intervals.

2.3. Analysis and statistics

All analyses were performed using custom MATLAB code. We blanked the stimulus artefact in the EMG recordings by interpolating between points that occurred 4 ms prior to and 6 ms after the stimulus onset. We filtered EMG data using a second order band pass filter with cutoff frequencies of 20 Hz and 1999 Hz.

We determined the latency of the PRM reflexes as the time from the stimulation onset to the first inflection of the response. Specifically, we detected when the amplitude of the evoked response exceeded one standard deviation beyond the mean baseline (pre-stimulus) period. We determined a reflex threshold value using data recorded for the recruitment curve: we defined the PRM reflex threshold as the stimulation amplitude where an evoked response was present in at least one of the four repetitions. We

determined the presence of a PRM reflex if the peak-to-peak amplitude of the evoked response exceeded five standard deviations beyond the mean baseline (pre-stimulus) period and confirmed this visually. We constructed recruitment curves by calculating the average of the four PRM reflex responses elicited at each stimulation amplitude. We then measured the peak-to-peak amplitude of the averaged responses according to stimulation charge. We found the slope of the recruitment curve by first using the MATLAB function *findchangepts* to find the inflection points. While implementing the *findchangepts* function, we set the maximum number of change points equal to two, and the minimum allowable number of samples equal to two. Then, we determined the slope of the line between those inflection points across the steepest part of the curve.

We created strength-duration curves for each waveform by finding the average threshold from the two repetitions at the same stimulation amplitude for each pulse duration. We created charge-duration curves by multiplying the threshold amplitude by the pulse duration, taking into account the duty cycle of the high-frequency carrier waveform. We performed a linear regression on the charge-duration curves. From the linear regression, we extracted the slope, which is equal to the rheobase (Reilly *et al* 1992, Lin *et al* 2002) (also the threshold amplitude at infinite duration). The y-intercept is equivalent to the minimum charge threshold for short pulses (duration approaching zero). Finally, we calculated the chronaxie by taking the quotient of the y-intercept and the slope. The chronaxie is also equivalent to the duration for two times the rheobase from the strength-duration curve.

We obtained discomfort scores at threshold as pulse duration was varied, and used the mean of the two scores for each pulse duration. There were no significant differences between the discomfort values across pulse durations (one-way analysis of variance (ANOVA); $p = 1.0$); therefore, we grouped the discomfort scores across pulse durations for comparisons.

We used paired t-tests to ascertain differences between the conventional and high-frequency carrier waveforms for the following measures: stimulation amplitudes at PRM reflex threshold, peak-to-peak amplitudes at threshold, PRM reflex latencies, decrease in peak-to-peak amplitude following RDD, recruitment rate, and discomfort scores. We used the two one-sided t-test (Lakens 2017, Rastogi 2017) to test for equality between the two waveforms for the discomfort scores at threshold and latency of the PRM reflexes. We also tested for effects of order (starting with either the conventional or high-frequency carrier waveform) on PRM reflex thresholds and comfort scores using paired t-tests. We performed a similar analysis with paired t-tests to determine if there were sex-based differences in PRM thresholds and comfort scores. Finally, we calculated the linear correlation coefficient between the threshold stimulation amplitude and the participant's waist and hip circumferences.

3. Results

We evoked PRM reflexes in all lower-limb muscles that were tested in all participants using both waveforms. For the purpose of reporting our main findings, we focus on the soleus muscle only (figures 2(A) and (B)) because the results from the other muscles were similar (supplementary figure 1). Near and above the PRM reflex threshold, large contractions in the paraspinal muscles occurred. The onset of paraspinal contractions and the induced trunk movements were a reliable indicator that the stimulation amplitude was likely to evoke a PRM reflex. In other words, if the participant's trunk moved during the stimulation pulse due to paraspinal contractions, the stimulation amplitude was also likely high enough to elicit a PRM reflex response. Although we did not ask participants to describe paresthesias, over half ($n = 10$) of them reported experiencing paresthesias in their ankles to toes. Furthermore, we observed movements in both legs in half ($n = 8$) of the participants.

3.1. The high-frequency carrier waveform required more charge to evoke PRM reflexes

The high-frequency carrier waveform required approximately double the charge (62.5 ± 11.1 μC) to evoke a PRM reflex compared to the conventional waveform (32.4 ± 9.2 μC), which was significant ($p < 0.001$; figure 2(C)). This equated to stimulation amplitudes of 125.1 ± 22.3 mA for the high-frequency carrier waveform and 32.4 ± 9.2 mA for the conventional waveform. The peak-to-peak amplitude of the PRM reflexes evoked at threshold by the high-frequency carrier waveform (33.1 ± 13.0) compared to the conventional waveform (34.8 ± 12.5) were not significantly different ($p = 0.32$; figure 2(D)). The latencies of the PRM reflexes (21.8 ± 1.9 and 22.0 ± 1.8 for the conventional and high-frequency carrier waveforms, respectively) were not significantly different ($p = 0.11$) and were equivalent with a window of $\pm 1.5\%$ ($p = 0.034$; figure 2(E)).

Neither the waist nor hip circumferences correlated with PRM reflex thresholds for either waveform ($R^2 < 0.1$; supplementary figure 2). Furthermore, sex did not influence the PRM reflex thresholds ($p > 0.5$; supplementary figure 5(A)). The order in which the waveforms were delivered also did not influence the PRM reflex threshold ($p > 0.35$; supplementary figure 5(C)).

3.2. PRM reflexes exhibited RDD

We confirmed that the evoked responses were reflexive by observing RDD. When the stimuli were 10 s

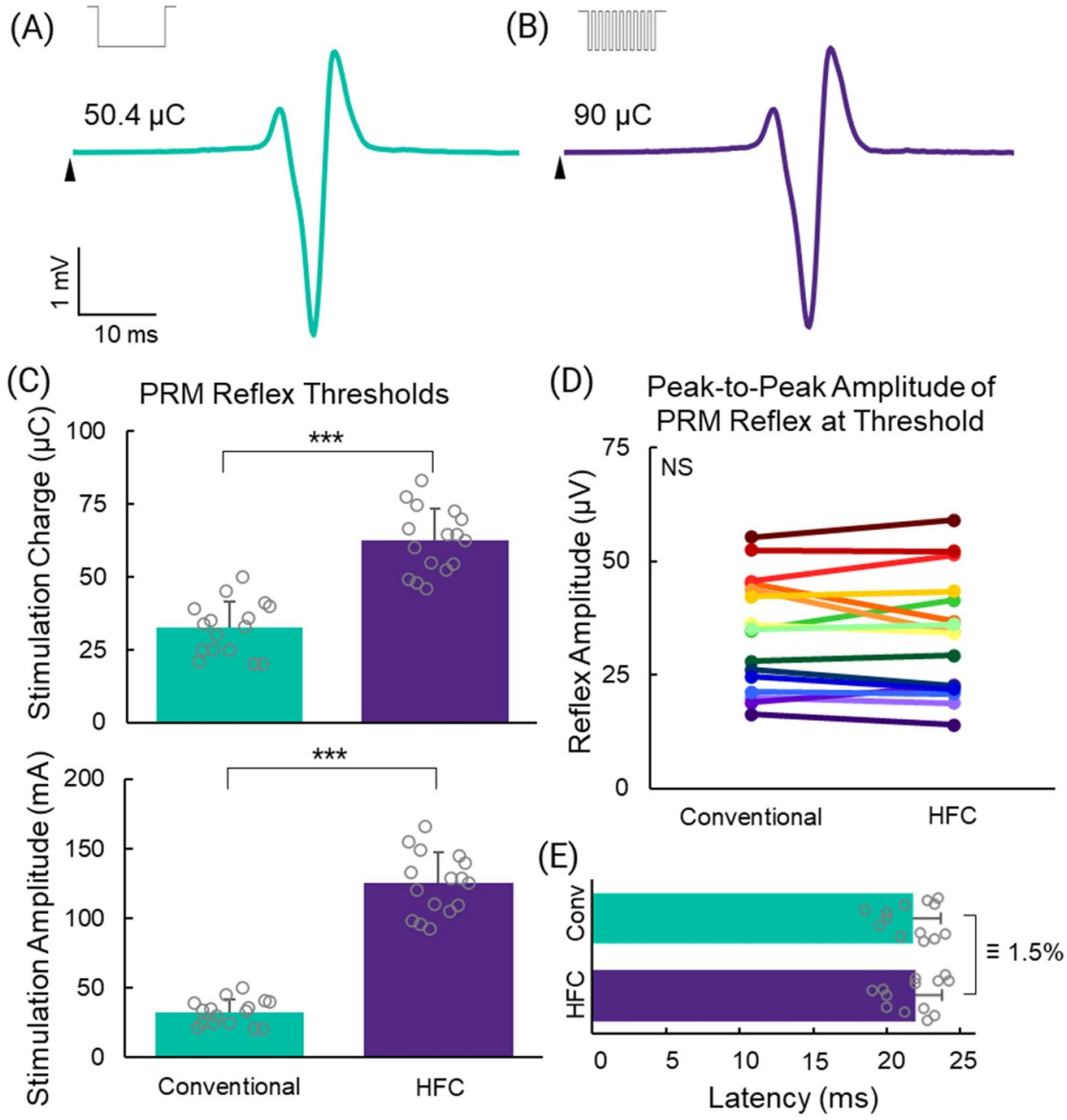

Figure 2. Posterior root muscle (PRM) reflexes from the soleus muscle of TSP08. Examples of PRM reflexes of the same peak-to-peak amplitude, evoked using the conventional (Conv) waveform at 50.4 μC (A) and the high-frequency carrier (HFC) waveform at 90 μC (B). The waveforms are indicated by the insets. The onset of stimulation is indicated by an arrow. (C) Comparison of PRM reflex thresholds using the conventional versus the high-frequency carrier waveform according to stimulation charge (top) and amplitude (bottom). (D) Comparison of the peak-to-peak amplitude of the PRM reflexes at threshold across all subjects. (E) Latency of the PRM reflexes. Error bars represent standard deviation; $^{***}p < 0.001$; NS = not significant; ≡1.5% indicates that the latencies were equivalent within a ±1.5% window.

apart, the peak-to-peak amplitude of the PRM reflex remained constant (figure 3(A)). When the interstimulus interval was 1 s, the peak-to-peak amplitude decreased with successive stimuli. This occurred for both waveforms (figures 3(B) and (C)). On average, the peak-to-peak amplitude of the second PRM reflex evoked by the conventional and high-frequency carrier waveforms were 47.5% (±23.9%) and 64.9% (±25.4%) of the first PRM reflex, respectively, and were not significantly different between waveforms ($p = 0.09$; figure 3(D)). In most cases, the peak-to-peak amplitude of the third PRM reflex was also depressed; however, in 9/32 instances, the peak-to-peak amplitude of the third PRM reflex increased to approximately that of the first response (supplementary figure 3).

3.3. Both waveforms had similar recruitment rates

We collected recruitment curves by varying the stimulation amplitude between subthreshold and supramaximal amplitudes (figures 4(A)–(C). The slope of the recruitment curve indicates the rate of activation of the PRM reflex. In most participants, the PRM_{Max} was not reached using the high-frequency carrier waveform. Therefore, the slope of the recruitment curve was calculated only if the high-frequency carrier PRM_{Max} was at least 33% of the conventional PRM_{Max} (occurred only in TSP01, TSP02, TSP04,

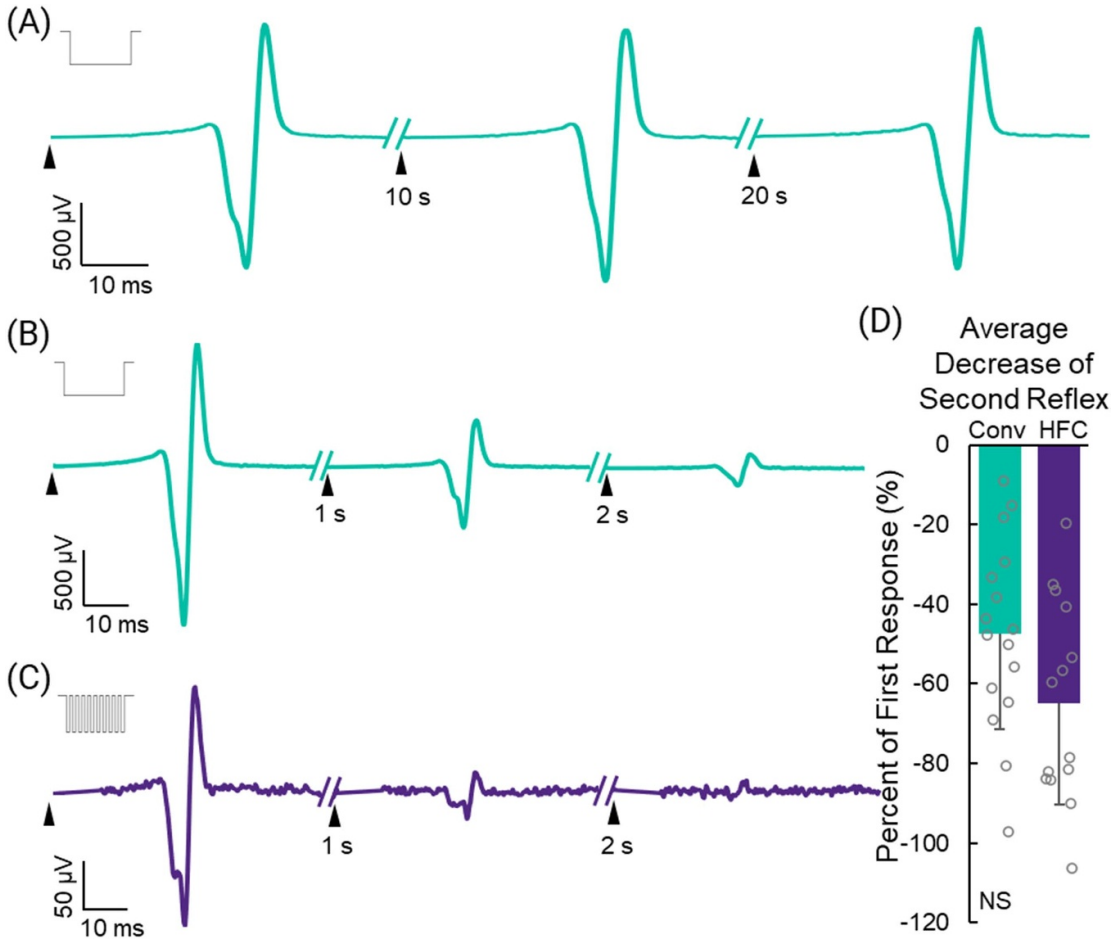

Figure 3. Rate-dependent depression. Example of posterior root muscle (PRM) reflexes following three consecutive stimulation pulses delivered 10 s apart (A), showing a constant peak-to-peak amplitude, or 1 s apart (B), (C), showing a decrease in the peak-to-peak amplitude of the successive responses. Stimulation amplitudes were set to ∼1.1–1.3× PRM threshold. All responses shown were recorded in the soleus muscle from TSP02. The type of waveform used in each subfigure is indicated by the inset. The onset of stimulation is indicated by an arrow. (D) Average (- standard deviation) of the peak-to-peak amplitude of the second PRM reflex as a percentage of the first PRM reflex in the series. HFC = high-frequency carrier; Conv = conventional.

and TSP08; supplementary figure 4). The recruitment rates for the conventional and high-frequency carrier waveforms were 0.39 ± 0.29 mV μC^{-1} and 0.28 ± 0.23 mV μC^{-1}, respectively, and were not significantly different ($p = 0.08$).

3.4. The waveforms were equally comfortable at PRM reflex threshold

At PRM reflex threshold, the mean discomfort score for the conventional and high-frequency carrier waveforms were 0.87 ± 0.2 and 1.03 ± 0.18, respectively, and were not significantly different from one another ($p = 0.13$), but were equivalent within a ±1% window ($p = 0.002$; figure 5(C)). Sex did not have an effect on the discomfort scores ($p > 0.25$; supplementary figure 5(B)), nor did the order of which waveform was tested first ($p > 0.55$; supplementary figures 5(D) and (E)).

As the stimulation charge increased, the contraction strength of paraspinal muscles were rated higher and increased linearly (conventional: $R^2 = 0.98$; high-frequency: $R^2 = 0.96$; figure 5(B)). We used the equations from linear regression to estimate the contraction score at PRM reflex threshold:

$$Score_{\mathrm{Conv}} = 0.0713 \times Thresh_{\mathrm{Conv}} - 0.6 \quad (1)$$

$$Score_{\mathrm{HF}} = 0.0267 \times Thresh_{\mathrm{HF}} - 0.2042. \quad (2)$$

At threshold, the contraction score for the conventional and high-frequency carrier waveforms were 1.71 and 1.46, respectively, indicating that they induced similarly strong paraspinal muscle contractions.

3.5. The high-frequency carrier waveform delivered charge less efficiently

The values for the rheobase, chronaxie, and minimum charge extracted from the charge-duration curves are listed in table 2 and labeled in figure 6. For six participants, the thresholds for narrower pulse durations were greater than 180 mA for the high-frequency carrier waveform. In most of these cases, only the narrowest point (100 μs) was outside of this bound; however, in one instance, the

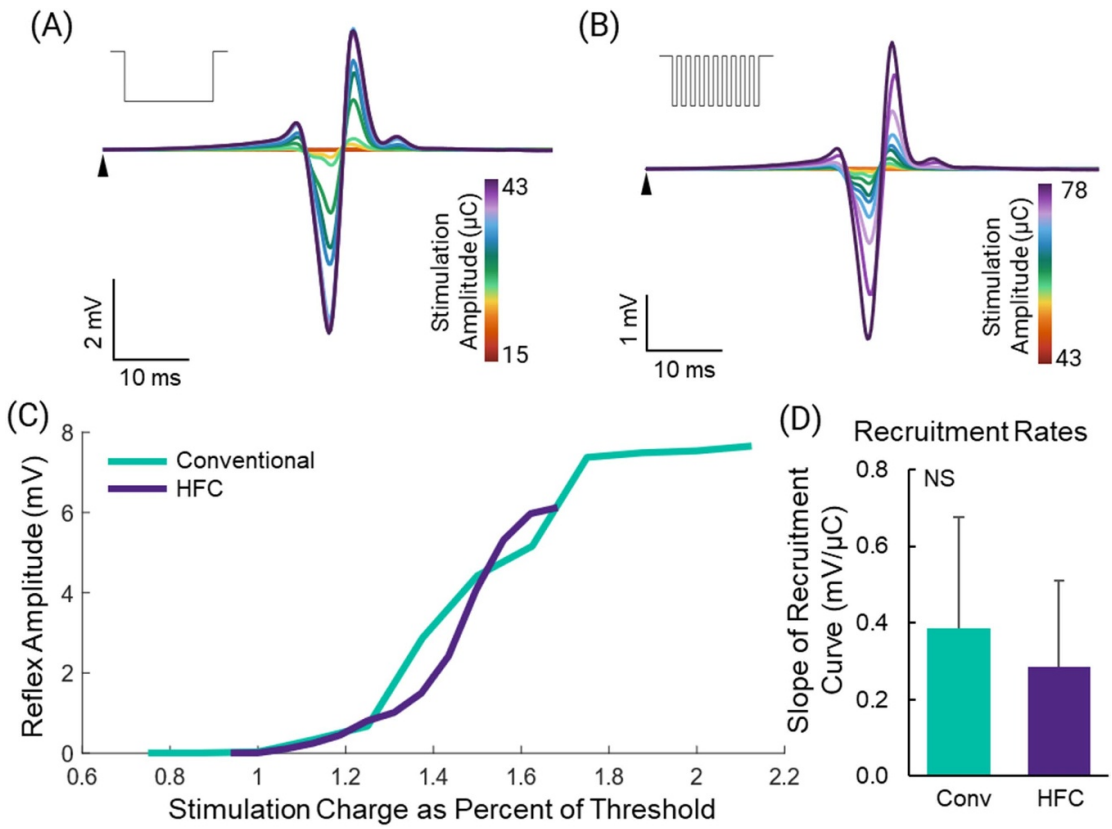

Figure 4. Recruitment of posterior root muscle (PRM) reflexes. PRM reflexes evoked across a range of amplitudes using the conventional (Conv) waveform (A) and the high-frequency carrier (HFC) waveform (B). The type of waveform used in each subfigure is indicated by the inset. The onset of stimulation is indicated by an arrow. (C) Peak-to-peak amplitude of the PRM reflex response plotted against the stimulation charge as a percent of threshold. All responses shown were recorded in the soleus muscle from TSP02. (D) Recruitment rates of PRM reflexes for instances where the maximum peak-to-peak amplitude from the HFC waveform was at least 33% of the maximum from the conventional waveform. Error bars represent standard deviation. $^{***}p < 0.001$; NS = not significant.

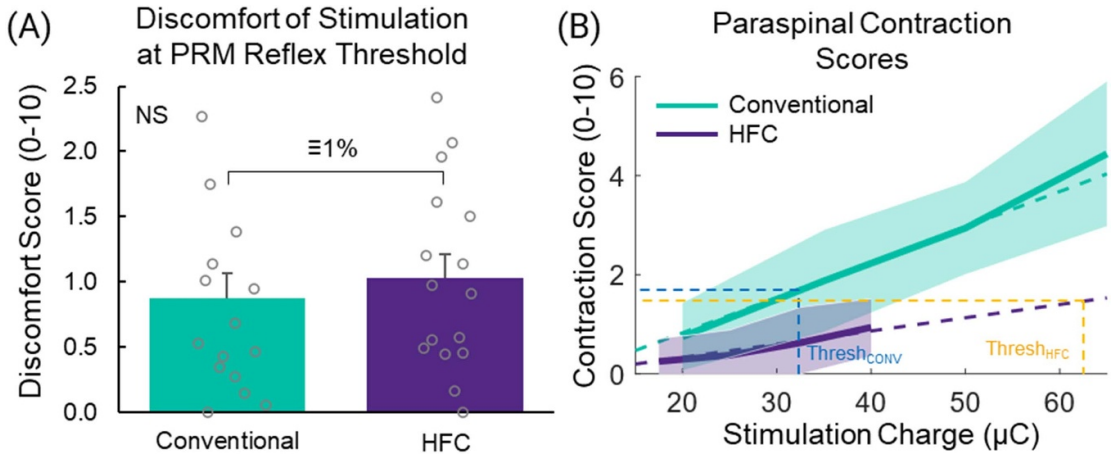

Figure 5. Discomfort and contraction scores. (A) Mean (+ standard deviation) of the scores for the discomfort felt at threshold along the strength-duration curves. (B) Mean (± standard deviation) scores for the paraspinal muscle contractions felt at each stimulation amplitude for each waveform. NS = not significant; HFC = high-frequency carrier; CONV = conventional; ≡1% indicates that the discomfort scores were equivalent within a ±1% window.

200 μs and 400 μs data points were outside this bound. Therefore, for pulse durations less than 400 μs, and in particular at 100 μs, the threshold value was underestimated, and these data points were removed from analysis. The strength-duration curve for the high-frequency carrier waveform can be duplicated by shifting the strength-duration curve for the conventional waveform up by 94.7 mA (supplementary figure 6) in a near perfect overlap (Correlation = 96.1%). These results demonstrate

Table 2. Parameters from charge-duration and strength-duration curves. The parameters were determined using a linear regression of the charge-duration curves for each waveform. HFC = high-frequency carrier.

Parameter	Conventional waveform	HFC waveform	HFC/Conventional
Rheobase (mA)	25.06	120.42	4.81
Chronaxie (μs)	292.1	51.4	0.18
Minimum charge (μC)	7.32	6.19	0.85

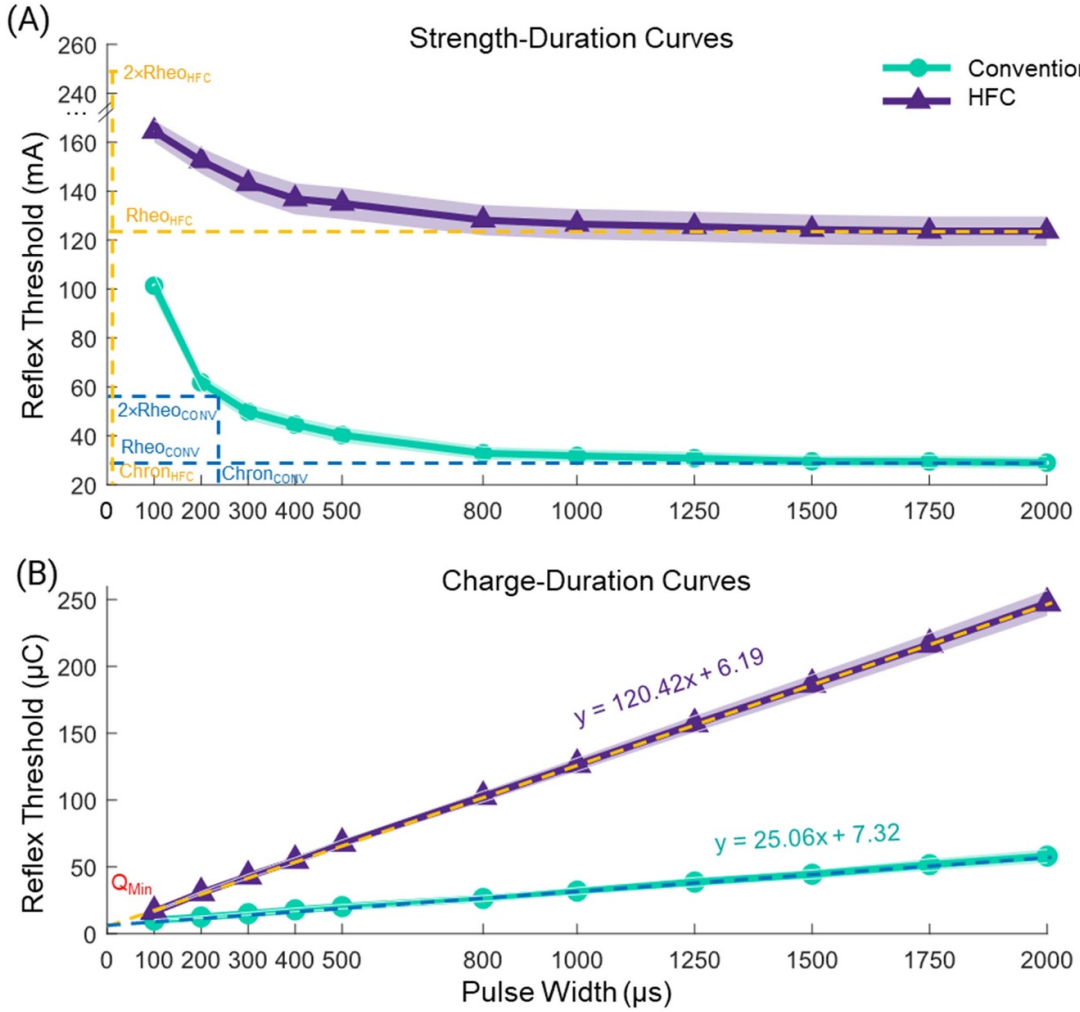

Figure 6. Strength- and charge-duration curves. (A) Mean (± standard error) threshold stimulation amplitude for evoking a posterior root muscle (PRM) reflex as the pulse duration was varied. Note: for the high-frequency carrier (HFC) waveform, the threshold for pulse durations <300 μs were >180 mA; therefore, the curve is incorrectly less steep. CONV = conventional waveform. (B) Mean (± standard error) charge threshold as pulse duration was varied. Q_{Min} = minimum charge; the equations are from linear regression.

that the high-frequency carrier waveform activates the same afferent fibers as the conventional waveform, but less efficiently.

4. Discussion

4.1. PRM reflexes

tSCS utilizes high stimulation current levels delivered through adhesive paravertebral electrodes to target the deep spinal roots, evoking PRM reflexes that can be recorded in the lower limb muscles. The thresholds did not differ across hip and waist circumferences, likely because the near midline placement of the tSCS electrode avoided areas of larger adipose or muscle tissue regions, allowing more direct access to the spinal nerves. tSCS neuromodulation for the recovery of motor functions requires stimulation amplitudes at or near PRM reflex threshold to be effective (Rath *et al* 2018, Sayenko *et al* 2019, Hofstoetter *et al* 2021, Inanici *et al* 2021, Keller *et al* 2021). PRM reflexes consist of a multi-segment superposition of H-reflexes and cutaneous afferent inputs (Minassian *et al* 2007,

Krenn *et al* 2013, Freitas *et al* 2022). A characteristic of spinal reflexes is the presence of RDD, indicated by the reduced amplitude of successive reflex responses following an initial pulse (Andrews *et al* 2015). We observed RDD at 1 Hz, verifying that the responses were reflexive, similar to data from a previous study (Hofstoetter *et al* 2019). We also reported periodic modulation of reflex amplitudes with further successive pulses. This behavior has been reported previously with eSCS in people with SCI (Hofstoetter *et al* 2015a). Our results suggest that both waveforms act through a similar reflex pathway, because the shapes of the responses were identical within each participant and muscle, and they had similar recruitment characteristics.

4.2. Discomfort of stimulation at PRM reflex threshold

Discomfort is a limitation of electrical stimulation, especially at high amplitudes in people with intact sensation. Activation of cutaneous nociceptors and paraspinal muscle contractions are the main causes of discomfort during tSCS. Both types of discomfort have been reported in several studies, including in people with SCI, sometimes requiring discontinuation for several days (Hofstoetter *et al* 2018, Manson *et al* 2020, Keller *et al* 2021). Our participants, who had intact sensation, reported strong paraspinal muscle contractions and discomfort of electrical stimulation at higher amplitudes. The discomfort experienced by people with motor disorders such as SCI will depend on the extent of sensation remaining at the stimulation site. However, therapeutic tSCS for motor recovery requires stimulation amplitudes at or below threshold (Hofstoetter *et al* 2015b, Rath *et al* 2018, Inanici *et al* 2021), where mild paraspinal contractions are produced. Our results show that, at threshold, the strength of contractions of the paraspinal muscles are similar and small.

A recent study from the Sayenko lab investigated the maximum tolerable stimulation amplitude for tSCS with and without a 5 kHz carrier frequency (Manson *et al* 2020). They noted that 70% of participants discontinued stimulation due to the discomfort of strong paraspinal contractions, 10% due to abdominal contractions (where their return electrode was located), and 20% due to stimulation-site discomfort. Participants could tolerate larger currents with high-frequency stimulation. However, when the maximum tolerable stimulation amplitude was normalized to the PRM reflex threshold, there was no difference between the waveforms. This showed that the reflex threshold and maximum tolerable stimulation amplitude scaled together with the addition of a high-frequency carrier. They concluded that high-frequency stimulation does not reduce discomfort at intensities needed to evoke PRM reflexes. Our results support this inference and explicitly demonstrate that, at PRM reflex threshold, which is relevant for tSCS neuromodulation applications, the addition of a 10 kHz carrier frequency does not reduce discomfort.

4.3. Mechanisms of high-frequency stimulation

A common claim to support the use of high-frequency tSCS is that it blocks local cutaneous afferents, resulting in painless stimulation (Gerasimenko *et al* 2015a, Gad *et al* 2017, Sayenko *et al* 2019, Manson *et al* 2020, Inanici *et al* 2021). The concept of conduction block has been prevalent for decades. In the 1960's, Tanner reported conduction block with 20 kHz stimulation, noting that large diameter fibers were blocked first (Tanner 1962). A computational model showed that both deep and superficial large diameter afferents are activated with high-frequency stimulation (Medina and Grill 2014). Lempka and colleagues used a computational model to show that high-frequency stimulation causes activation and blocking of axons, both in larger diameter fibers first (Lempka *et al* 2015). Specifically, nerve fibers were activated at lower thresholds but blocked at amplitudes greater than the clinical range for eSCS. It has also been demonstrated experimentally that 10 kHz stimulation blocked large diameter afferents at lower amplitudes than for unmyelinated fibers, which required supraclinical amplitudes (Joseph and Butera 2011). Blocking may dominate when high-frequency stimulation is delivered tonically (Ward *et al* 2004, Bhadra *et al* 2018), but only after eliciting a large initial response (Ackermann *et al* 2011). tSCS neuromodulation delivers stimulation in bursts of high-frequency trains, typically at 30–50 Hz, which may have different blocking properties than tonic stimulation. If blocking does occur during tSCS, the large diameter fibers would be blocked before small diameter fibers. Given that single bursts of high-frequency stimulation are equally as comfortable as a conventional pulse and the known blocking properties of the different afferent fibers, the notion that high-frequency tSCS blocks local cutaneous afferents but activates deep spinal roots is likely incorrect.

Over half our participants experienced paresthesias in their lower limbs using either waveform. Paresthesias are thought to indicate activation of Aβ mechanoreceptors (Caylor *et al* 2019, Rogers *et al* 2022) and have been reported in previous tSCS studies using the conventional waveform (Hofstoetter *et al* 2015b, 2021). High-frequency stimulation is used in some forms of eSCS for pain treatment. In this embodiment, high-frequency stimulation is referred to as 'paresthesia-free' (Sdrulla *et al* 2018, Caylor *et al* 2019); however, eSCS is applied tonically, not in bursts of trains like tSCS. Whether or not Aβ fibers are activated using paresthesia-free eSCS remains unclear (Song *et al* 2014, Crosby *et al* 2017, Sdrulla *et al* 2018, Freitas *et al* 2022, Rogers *et al* 2022). The presence of paresthesias and the question of blocking indicate that further studies are needed to differentiate

the fibers being activated not only by different waveforms, but also when they are applied in single pulses, trains, or continuously.

Strength-duration curves describe activation of excitable tissues, where less excitable tissues are found higher and to the right of more excitable tissues. Here, the high-frequency carrier strength-duration curve was a direct copy of the conventional strength-duration curve, shifted up but not right, suggesting that both waveforms activated the same afferent fibers. The rheobase indicates the absolute minimum current required to activate a nerve fiber, and the chronaxie is a function of the axon membrane time constant, which corresponds to excitability (Reilly *et al* 1992, Lin *et al* 2002). The rheobase for the high-frequency carrier waveform was nearly five times greater than the conventional waveform, and the chronaxie more than five times narrower. High-frequency stimulation causes nerve excitation through summation, where each brief pulse in the burst brings the membrane closer to threshold, eventually leading to an action potential (Ward *et al* 2004, Ward and Lucas-Toumbourou 2007). Since the high-frequency carrier waveform had a 50% duty cycle, one would expect the rheobase to be twice that of the conventional waveform. Our results show that integration does occur over the duration of the high-frequency pulse, but the summation is leaky, requiring significantly higher levels of current to achieve threshold than is required of the conventional waveform. This leaky summation results in less efficient excitation of afferent fibers, unnecessary charge injection, and excessive current consumption (Irnich 1980), which reduces the lifetime of battery-powered devices, and could lead to electrode degradation as well as local tissue heating.

4.4. Study limitations

The upper limit for the stimulation current in this study was 180 mA. We chose this limit based on other tSCS studies. A few papers tested stimulation amplitudes up to 200 mA in people with SCI (Gerasimenko *et al* 2015a, Gad *et al* 2017, 2018); a recent study stimulated as high as 1000 mA in neurologically intact individuals without adverse events (Manson *et al* 2020). The primary focus of our study was to investigate the comfort of each waveform at threshold for evoked PRM reflexes; therefore, the behavior at higher stimulation amplitudes was less critical.

We used a monophasic stimulation pulse, because monophasic pulses are typically used for reflex studies (Sayenko *et al* 2015, Burke 2016, Murray and Knikou 2019). Many tSCS neuromodulation studies use monophasic pulses (Minassian *et al* 2016, Gad *et al* 2018, Knikou and Murray 2019, Sayenko *et al* 2019, Wu *et al* 2020). Biphasic stimulation is likely to have a higher threshold than monophasic stimulation (Reilly *et al* 1992), but should be confirmed in a study comparing PRM reflex activation with monophasic versus biphasic pulses. Furthermore, tSCS for neuromodulation is applied continuously, in contrast to the single, 1 ms-long pulses used for studying reflexes. The tolerance of continuous stimulation at PRM reflex threshold should be investigated in future studies.

Posture and leg position can affect PRM reflex thresholds. We evoked PRM reflexes while our participants sat comfortably in a chair, with their knees positioned at a 120° angle, to avoid postural effects on tSCS thresholds. In one study investigating postural effects on PRM reflex thresholds, they found that PRM reflexes had a much greater threshold while lying prone compared to supine, and the lowest thresholds were found while standing (Danner *et al* 2016). These posture-related influences on PRM reflex recruitment must be considered when tSCS is used as a neuromodulation method, especially during tasks that require the participant to move.

4.5. Implications for future studies and clinical translation

Therapeutic eSCS and tSCS use trains of stimulation pulses, often applied at 30–50 Hz, which is quite different than the single pulse applied in this study. A recent study reported that continuous trains of tSCS (30 Hz) were tolerated at only 15% of the current for a single pulse, which was 56% of motor threshold (Manson *et al* 2020). This seems to contradict the numerous reports of using tSCS neuromodulation in people with intact sensation at just below (Rath *et al* 2018, Hofstoetter *et al* 2020, 2021, Inanici *et al* 2021) or above (Gerasimenko *et al* 2015a, Gad *et al* 2018) motor threshold. We as a field need to understand the recruitment properties and comfort of single-pulse and continuous trains of tSCS to better understand how it engages with spinal reflex pathways during neuromodulation. Similar studies should be undertaken for other neuromodulation methods as well.

5. Conclusions

tSCS neuromodulation for motor recovery requires stimulation amplitudes near PRM reflex threshold to engage spinal reflex pathways. Using a high-frequency carrier for tSCS is less efficient and requires more charge to evoke PRM reflexes than a conventional monophasic stimulation pulse. At reflex thresholds, high-frequency carrier stimulation is not more comfortable than conventional stimulation, despite several claims of pain-free stimulation when a high-frequency carrier is used. While tSCS offers a non-invasive approach to neuromodulation of motor output in the spinal cord, results from this study

discourage using a high-frequency carrier because it leads to unnecessarily high levels of charge to be applied.

Data availability statement

The data that support the findings of this study are available upon reasonable request from the authors.

Acknowledgments

Thank you to Axelgaard Manufacturing Co., Ltd. for providing electrode samples to complete this work. We would also like to thank our research subjects for their commitment to science and willingness to participate in this study. We appreciate the feedback we received from our Data Safety and Monitoring Board throughout the completion of this study.

Funding source

This study was funded by the Department of Mechanical Engineering and the Neuroscience Institute at Carnegie Mellon University.

Author contributions

A N D, M C, and D J W conceived of the study; A N D and D J W designed the study; A N D collected and analyzed all data; C A H and M G K analyzed portions of the data; A N D, MC, and D J W interpreted the data; A N D, C A H, and M G K created the figures; A N D wrote the first draft of the manuscript; all authors refined and approved the final manuscript prior to submission.

Conflict of interest

M C and D J W are founders and shareholders of Reach Neuro, Inc.; D J W is a consultant and shareholder of Neuronoff, Inc.; D J W is a shareholder and scientific board member for NeuroOne Medical, Inc.; D J W is a shareholder of Bionic Power Inc., Iota Biosciences Inc., and Blackfynn Inc. The other authors declare no conflicts of interests in relation to this work.

ORCID iDs

Ashley N Dalrymple https://orcid.org/0000-0001-8566-7178
Charli Ann Hooper https://orcid.org/0000-0001-7466-7893
Minna G Kuriakose https://orcid.org/0000-0002-4738-5054
Marco Capogrosso https://orcid.org/0000-0002-0975-316X
Douglas J Weber https://orcid.org/0000-0002-9782-3497

References

Ackermann D M, Bhadra N, Foldes E L and Kilgore K L 2011 Conduction block of whole nerve without onset firing using combined high frequency and direct current *Med. Biol. Eng. Comput.* **49** 241–51
Andrews J C, Stein R B and Roy F D 2015 Post-activation depression in the human soleus muscle using peripheral nerve and transcutaneous spinal stimulation *Neurosci. Lett.* **589** 144–9
Angeli C A, Boakye M, Morton R A, Vogt J, Benton K, Chen Y, Ferreira C K and Harkema S J 2018 Recovery of over-ground walking after chronic motor complete spinal cord injury *N. Engl. J. Med.* **379** 1244–50
Bhadra N, Foldes E, Vrabec T, Kilgore K and Bhadra N 2018 Temporary persistence of conduction block after prolonged kilohertz frequency alternating current on rat sciatic nerve *J. Neural. Eng.* **15** 016012
Burke D 2016 Clinical uses of H reflexes of upper and lower limb muscles *Clin. Neurophysiol. Pract.* **1** 9–17
Calvert J S, Manson G A, Grahn P J and Sayenko D G 2019 Preferential activation of spinal sensorimotor networks via lateralized transcutaneous spinal stimulation in neurologically intact humans *J. Neurophysiol.* **122** 2111–8
Capogrosso M, Wenger N, Raspopovic S, Musienko P, Beauparlant J, Bassi Luciani L, Courtine G and Micera S 2013 A computational model for epidural electrical stimulation of spinal sensorimotor circuits *J. Neurosci.* **33** 19326–40
Carhart M R, He J, Herman R, D'Luzansky S and Willis W T 2004 Epidural spinal-cord stimulation facilitates recovery of functional walking following incomplete spinal-cord injury *IEEE Trans. Neural Syst. Rehabil. Eng.* **12** 32–42
Caylor J *et al* 2019 Spinal cord stimulation in chronic pain: evidence and theory for mechanisms of action *Bioelectron. Med.* **5** 12
Crosby N D, Janik J J and Grill W M 2017 Modulation of activity and conduction in single dorsal column axons by kilohertz-frequency spinal cord stimulation *J. Neurophysiol.* **117** 136–47
Danner S M, Krenn M, Hofstoetter U S, Toth A, Mayr W and Minassian K 2016 Body position influences which neural structures are recruited by lumbar transcutaneous spinal cord stimulation *PLoS One* **11** e0147479
Freitas R M, De, Capogrosso M, Nomura T and Milosevic M 2022 Preferential activation of proprioceptive and cutaneous sensory fibers compared to motor fibers during cervical transcutaneous spinal cord stimulation: a computational study *J. Neural. Eng.* **19** 036012
Freyvert Y, Yong N A, Morikawa E, Zdunowski S, Sarino M E, Gerasimenko Y, Edgerton V R and Lu D C 2018 Engaging cervical spinal circuitry with non-invasive spinal stimulation and buspirone to restore hand function in chronic motor complete patients *Sci. Rep.* **8** 1–10
Gad P, Gerasimenko Y and Edgerton V R 2019 Tetraplegia to overground stepping using non-invasive spinal neuromodulation *2019 9th Int. IEEE/EMBS Conf. on Neural Engineering (NER)* pp 89–92
Gad P, Gerasimenko Y, Zdunowski S, Turner A, Sayenko D, Lu D C and Edgerton V R 2017 Weight bearing over-ground stepping in an exoskeleton with non-invasive spinal cord neuromodulation after motor complete paraplegia *Front. Neurosci.* **11**
Gad P, Lee S, Terrafranca N, Zhong H, Turner A, Gerasimenko Y and Edgerton V R 2018 Non-invasive activation of cervical spinal networks after severe paralysis *J. Neurotrauma* **35** 2145–58
Gerasimenko Y P *et al* 2015b Noninvasive reactivation of motor descending control after paralysis *J. Neurotrauma* **32** 1968–80
Gerasimenko Y *et al* 2016 Integration of sensory, spinal, and volitional descending inputs in regulation of human locomotion *J. Neurophysiol.* **116** 98–105

Gerasimenko Y, Gorodnichev R, Moshonkina T, Sayenko D, Gad P and Reggie Edgerton V 2015a Transcutaneous electrical spinal-cord stimulation in humans *Ann. Phys. Rehabil. Med.* **58** 225–31

Gill M L *et al* 2018 Neuromodulation of lumbosacral spinal networks enables independent stepping after complete paraplegia *Nat. Med.* **24** 1677–82

Harkema S *et al* 2011 Effect of epidural stimulation of the lumbosacral spinal cord on voluntary movement, standing, and assisted stepping after motor complete paraplegia: a case study *Lancet* **377** 1938–47

Hofstoetter U S, Danner S M, Freundl B, Binder H, Mayr W, Rattay F and Minassian K 2015a Periodic modulation of repetitively elicited monosynaptic reflexes of the human lumbosacral spinal cord *J. Neurophysiol.* **114** 400–10

Hofstoetter U S, Freundl B, Binder H and Minassian K 2018 Common neural structures activated by epidural and transcutaneous lumbar spinal cord stimulation: elicitation of posterior root-muscle reflexes *PLoS One* **13** e0192013

Hofstoetter U S, Freundl B, Binder H and Minassian K 2019 Recovery cycles of posterior root-muscle reflexes evoked by transcutaneous spinal cord stimulation and of the H reflex in individuals with intact and injured spinal cord *PLoS One* **14** e0227057

Hofstoetter U S, Freundl B, Danner S M, Krenn M J, Mayr W, Binder H and Minassian K 2020 Transcutaneous spinal cord stimulation induces temporary attenuation of spasticity in individuals with spinal cord injury *J. Neurotrauma* **37** 481–93

Hofstoetter U S, Freundl B, Lackner P and Binder H 2021 Transcutaneous spinal cord stimulation enhances walking performance and reduces spasticity in individuals with multiple sclerosis *Brain Sci.* **11** 472

Hofstoetter U S, Hofer C, Kern H, Danner S M, Mayr W, Dimitrijevic M R and Minassian K 2013 Effects of transcutaneous spinal cord stimulation on voluntary locomotor activity in an incomplete spinal cord injured individual *Biomed. Eng. Biomed. Tech.* **58** 1–3

Hofstoetter U S, Krenn M, Danner S M, Hofer C, Kern H, McKay W B, Mayr W and Minassian K 2015b Augmentation of voluntary locomotor activity by transcutaneous spinal cord stimulation in motor-incomplete spinal cord-injured individuals *Artif. Organs* **39** E176–86

Hofstoetter U S, McKay W B, Tansey K E, Mayr W, Kern H and Minassian K 2014 Modification of spasticity by transcutaneous spinal cord stimulation in individuals with incomplete spinal cord injury *J. Spinal Cord Med.* **37** 202–11

Inanici F, Brighton L N, Samejima S, Hofstetter C P and Moritz C T 2021 Transcutaneous spinal cord stimulation restores hand and arm function after spinal cord injury *IEEE Trans. Neural Syst. Rehabil. Eng.* **29** 310–9

Inanici F, Samejima S, Gad P, Edgerton V R, Hofstetter C P and Moritz C T 2018 Transcutaneous electrical spinal stimulation promotes long-term recovery of upper extremity function in chronic tetraplegia *IEEE Trans. Neural Syst. Rehabil. Eng.* **26** 1272–8

Irnich W 1980 The chronaxie time and its practical importance *Pacing Clin. Electrophysiol.* **3** 292–301

Joseph L and Butera R J 2011 High-frequency stimulation selectively blocks different types of fibers in frog sciatic nerve *IEEE Trans. Neural Syst. Rehabil. Eng.* **19** 550–7

Keller A, Singh G, Sommerfeld J H, King M, Parikh P, Ugiliweneza B, D'Amico J, Gerasimenko Y and Behrman A L 2021 Noninvasive spinal stimulation safely enables upright posture in children with spinal cord injury *Nat. Commun.* **12** 5850

Knikou M and Murray L M 2019 Repeated transspinal stimulation decreases soleus H-reflex excitability and restores spinal inhibition in human spinal cord injury *PLoS One* **14** e0223135

Krenn M, Toth A, Danner S M, Hofstoetter U S, Minassian K and Mayr W 2013 Selectivity of transcutaneous stimulation of lumbar posterior roots at different spinal levels in humans *Biomed. Tech.* **58** 1

Lakens D 2017 Equivalence tests: a practical primer for t tests, correlations, and meta-analyses *Soc. Psychol. Personal. Sci.* **8** 355–62

Lempka S F, McIntyre C C, Kilgore K L and Machado A G 2015 Computational analysis of kilohertz frequency spinal cord stimulation for chronic pain management *Anesthesiology* **122** 1362–76

Lin C S-Y, Chan J H L, Pierrot-Deseilligny E and Burke D 2002 Excitability of human muscle afferents studied using threshold tracking of the H reflex *J. Physiol.* **545** 661–9

Manson G A, Calvert J S, Ling J, Tychhon B, Ali A and Sayenko D G 2020 The relationship between maximum tolerance and motor activation during transcutaneous spinal stimulation is unaffected by the carrier frequency or vibration *Physiol. Rep.* **8** e14397

Medina L E and Grill W M 2014 Volume conductor model of transcutaneous electrical stimulation with kilohertz signals *J. Neural. Eng.* **11** 066012

Minassian K, Hofstoetter U S, Danner S M, Mayr W, Bruce J A, McKay W B and Tansey K E 2016 Spinal rhythm generation by step-induced feedback and transcutaneous posterior root stimulation in complete spinal cord-injured individuals *Neurorehabil. Neural Repair* **30** 233–43

Minassian K, Persy I, Rattay F, Dimitrijevic M R, Hofer C and Kern H 2007 Posterior root-muscle reflexes elicited by transcutaneous stimulation of the human lumbosacral cord *Muscle Nerve* **35** 327–36

Murray L M and Knikou M 2019 Transspinal stimulation increases motoneuron output of multiple segments in human spinal cord injury *PLoS One* **14** e0213696

Powell M P *et al* 2022 Epidural stimulation of the cervical spinal cord improves voluntary motor control in post-stroke upper limb paresis p 22273635 (available at: www.medrxiv.org/content/10.1101/2022.04.11.22273635v1) (Accessed 21 July 2022)

Rastogi A 2017 Two one-sided test (TOST) for equivalence (available at: www.mathworks.com/matlabcentral/fileexchange/63204-tost-sample1-sample2-d1-d2-alpha) (Accessed 27 September 2021)

Rath M, Vette A H, Ramasubramaniam S, Li K, Burdick J, Edgerton V R, Gerasimenko Y P and Sayenko D G 2018 Trunk stability enabled by noninvasive spinal electrical stimulation after spinal cord injury *J. Neurotrauma* **35** 2540–53

Reilly J P, Antoni H, Chilbert M A, Skuggevig W and Sweeney J D 1992 *Electrical Stimulation and Electropathology* (Cambridge: Cambridge University Press)

Rogers E R, Zander H J and Lempka S F 2022 Neural recruitment during conventional, burst, and 10 kHz spinal cord stimulation for pain *J. Pain* **23** 434–49

Rowald A *et al* 2022 Activity-dependent spinal cord neuromodulation rapidly restores trunk and leg motor functions after complete paralysis *Nat. Med.* **28** 260–71

Samejima S, Caskey C D, Inanici F, Shrivastav S R, Brighton L N, Pradarelli J, Martinez V, Steele K M, Saigal R and Moritz C T 2022 Multisite transcutaneous spinal stimulation for walking and autonomic recovery in motor-incomplete tetraplegia: a single-subject design *Phys. Ther.* **102** pzab228

Sayenko D G, Atkinson D A, Floyd T C, Gorodnichev R M, Moshonkina T R, Harkema S J, Edgerton V R and Gerasimenko Y P 2015 Effects of paired transcutaneous electrical stimulation delivered at single and dual sites over lumbosacral spinal cord *Neurosci. Lett.* **609** 229–34

Sayenko D G, Rath M, Ferguson A R, Burdick J W, Havton L A, Edgerton V R and Gerasimenko Y P 2019 Self-assisted standing enabled by non-invasive spinal stimulation after spinal cord injury *J. Neurotrauma* **36** 1435–50

Sdrulla A D, Guan Y and Raja S N 2018 Spinal cord stimulation: clinical efficacy and potential mechanisms *Pain Pract.* **18** 1048–67

Shealy C N, Mortimer J T and Reswick J B 1967 Electrical inhibition of pain by stimulation of the dorsal columns: preliminary clinical report *Anesth. Analg.* **46** 489–91

Song Z, Viisanen H, Meyerson B A, Pertovaara A and Linderoth B 2014 Efficacy of kilohertz-frequency and conventional spinal cord stimulation in rat models of different pain conditions *Neuromodulation Technol. Neural Interface* **17** 226–35

Tanner J A 1962 Reversible blocking of nerve conduction by alternating-current excitation *Nature* **195** 712–3

Ward A R and Lucas-Toumbourou S 2007 Lowering of sensory, motor, and pain-tolerance thresholds with burst duration using kilohertz-frequency alternating current electric stimulation *Arch. Phys. Med. Rehabil.* **88** 1036–41

Ward A R and Robertson V J 1998 Sensory, motor, and pain thresholds for stimulation with medium frequency alternating current *Arch. Phys. Med. Rehabil.* **79** 273–8

Ward A R, Robertson V J and Ioannou H 2004 The effect of duty cycle and frequency on muscle torque production using kilohertz frequency range alternating current *Med. Eng. Phys.* **26** 569–79

Ward A R and Shkuratova N 2002 Russian electrical stimulation: the early experiments *Phys. Ther.* **82** 1019–30

Wu Y-K *et al* 2020 Posteroanterior cervical transcutaneous spinal stimulation targets ventral and dorsal nerve roots *Clin. Neurophysiol. Pract.* **131** 451–60

SUPPLEMENTARY FIGURES

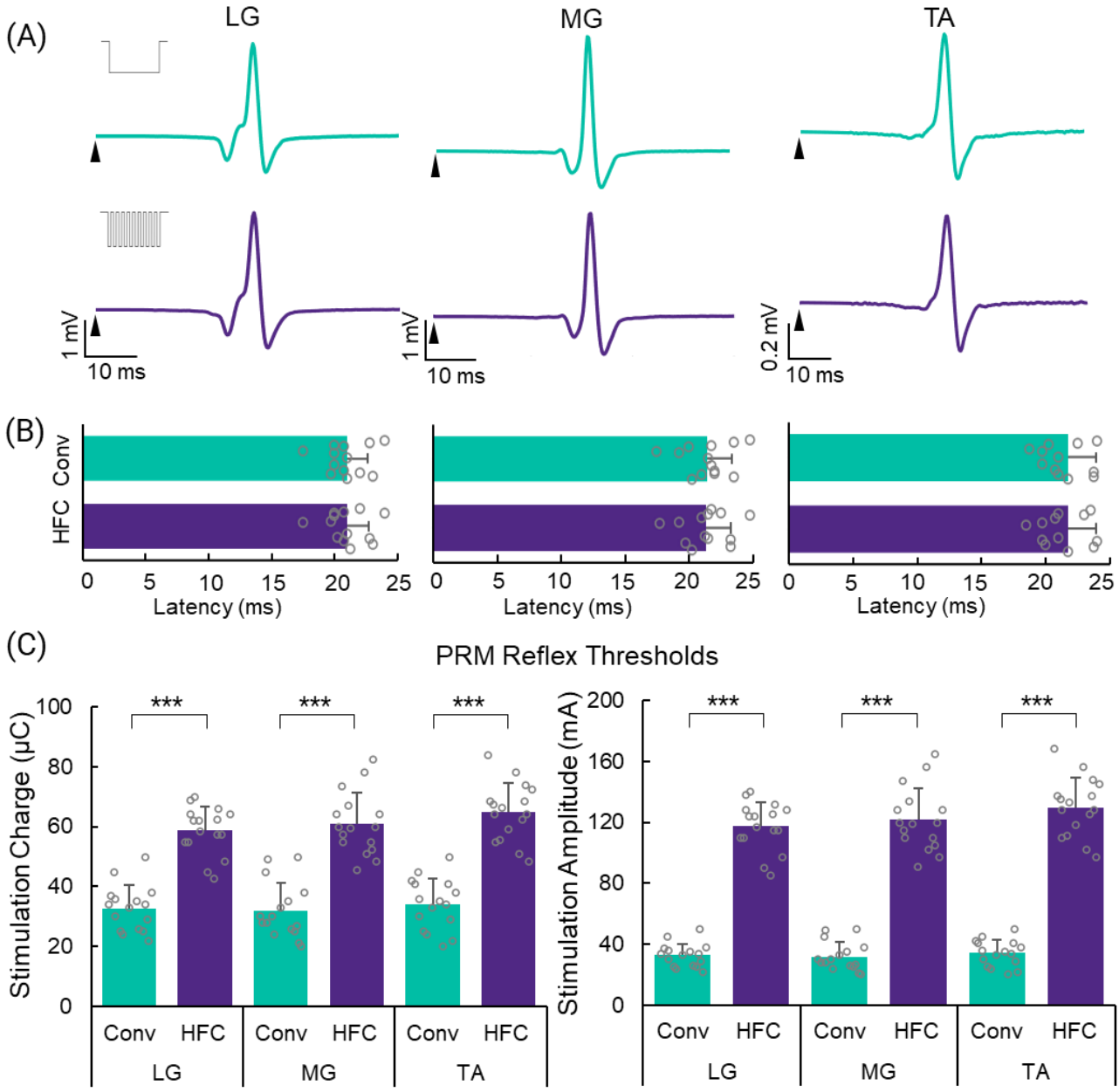

Supplementary Figure 1. Posterior root-muscle (PRM) reflexes in other lower leg muscles. (A) Examples of identical PRM reflexes evoked by each waveform (indicated by inset) for the lateral gastrocnemius (LG), medial gastrocnemius (MG), and tibialis anterior (TA) muscles. The onset of stimulation is indicated by an arrow. (B) Latency of PRM reflexes for each muscle and waveform. (C) PRM reflex thresholds for each muscle and waveform expressed in stimulation charge (left) and current (right). HFC = high-frequency carrier; Conv = conventional; error bars represent standard deviation; ***p < 0.001.

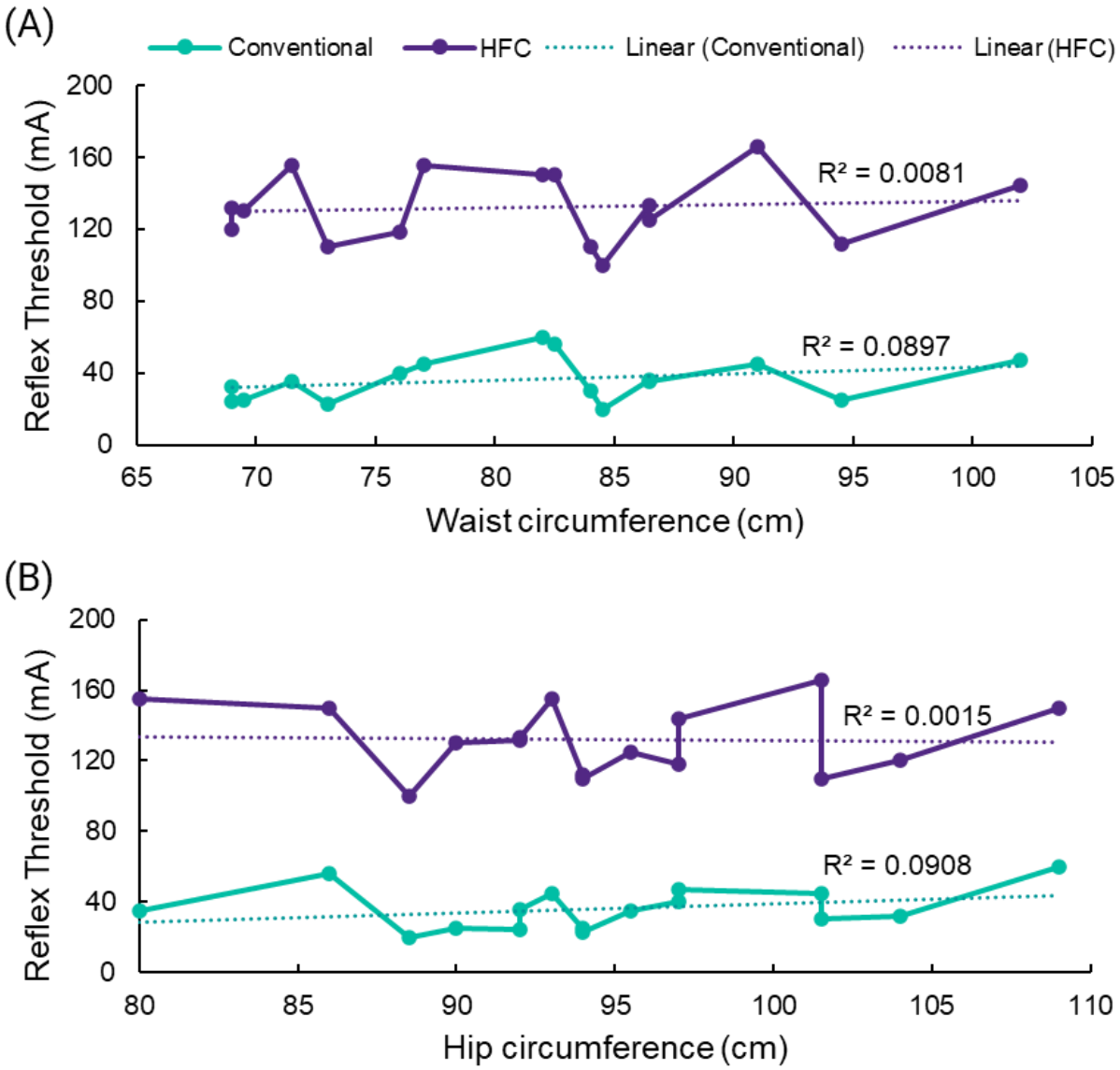

Supplementary Figure 2. Effect of size on thresholds. Posterior root-muscle (PRM) reflex threshold as a function of waist circumference (A) and hip circumference (B). Linear correlations are shown by the dotted lines.

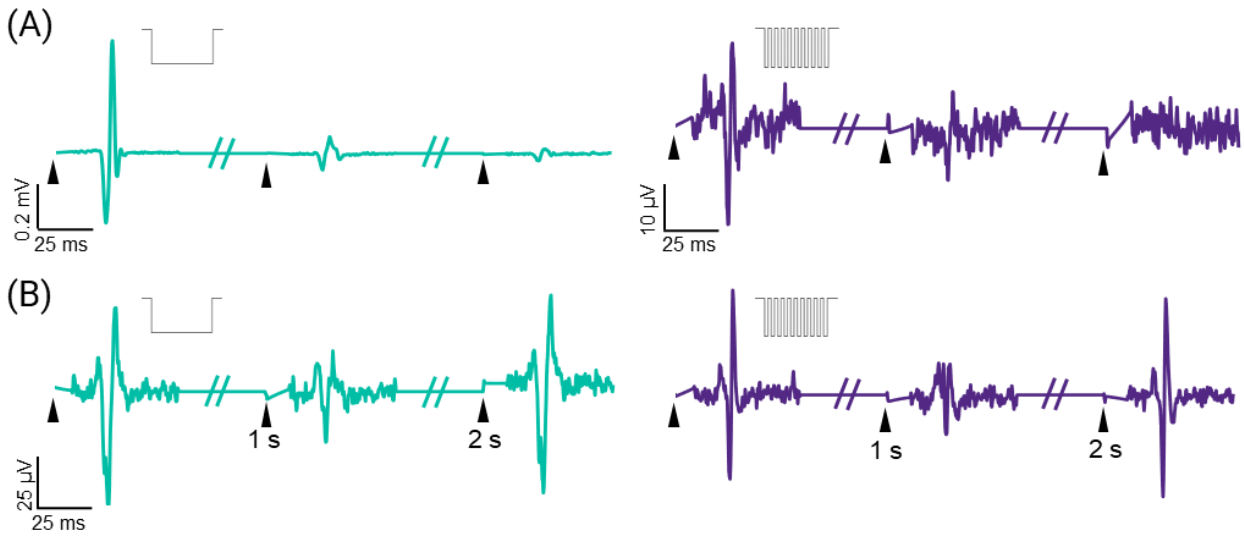

Supplementary Figure 3. Additional examples of rate-dependent depression of posterior root-muscle (PRM) reflexes. (A) Successive depression of PRM reflexes in the lateral gastrocnemius muscle in TSP02. (B) Periodic modulation of PRM reflexes in the soleus muscles of TSP16 (left) and TSP12 (right). The type of waveform used in each subfigure is indicated by the inset. The onset of stimulation is indicated by an arrow.

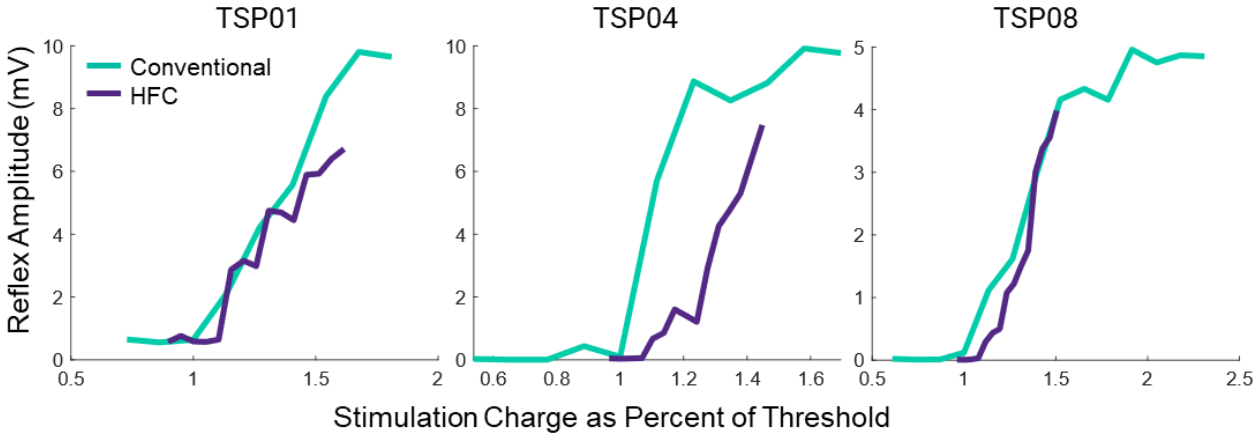

Supplementary Figure 4. Additional examples of recruitment curves from the soleus muscle where the maximum peak-to-peak amplitude of the posterior root-muscle (PRM) reflex evoked by the high-frequency carrier (HFC) waveform was at least 33% of the maximum peak-to-peak amplitude of the PRM reflex of the conventional waveform. This occurred only in TSP01, TSP02 (shown in Figure 4), TSP04, and TSP08. The peak-to-peak amplitude of the PRM reflex is response plotted against the stimulation charge as a percent of PRM reflex threshold.

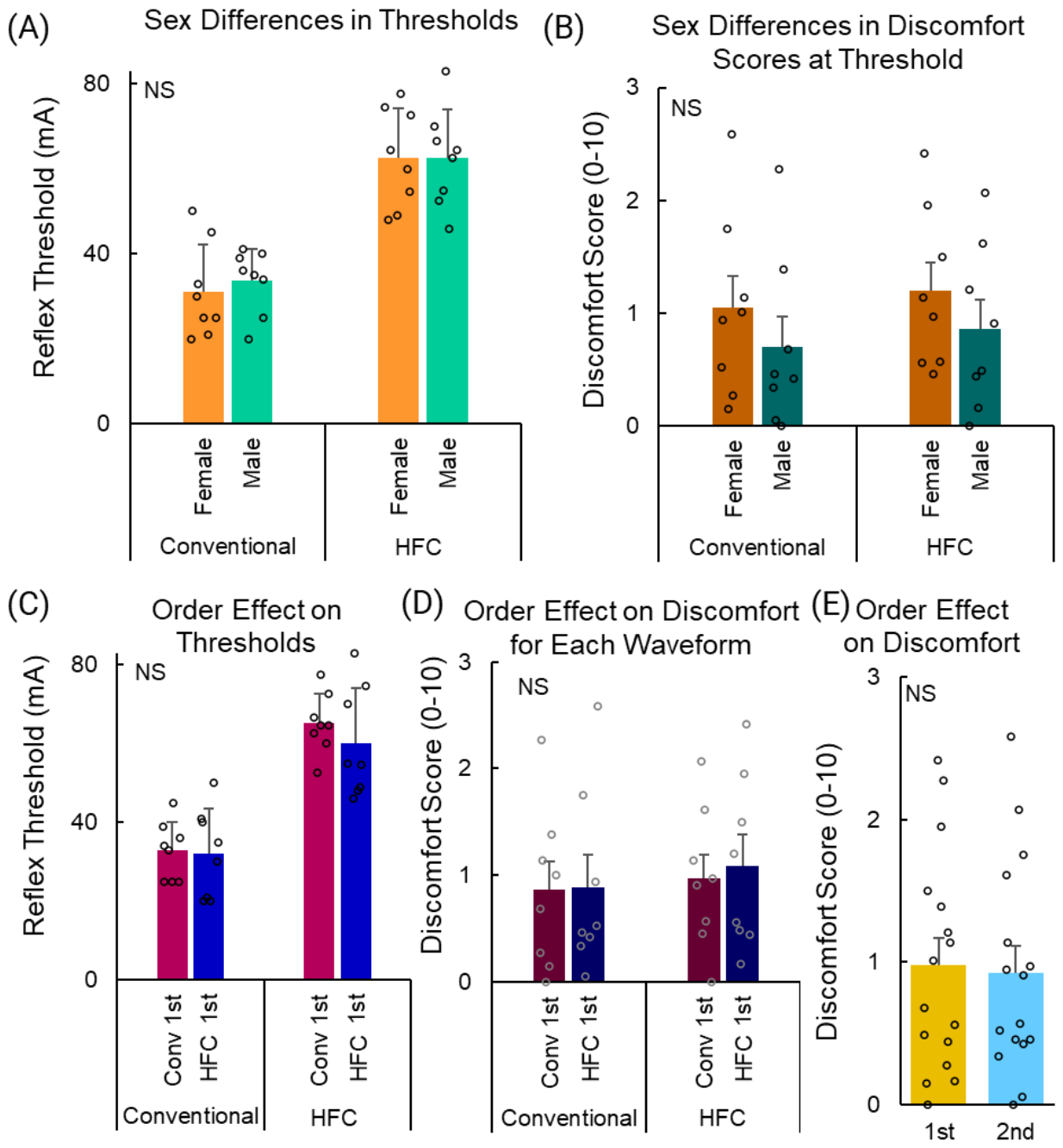

Supplementary Figure 5. Effects of sex and order on thresholds and comfort. Effect of sex on posterior root-muscle (PRM) reflex threshold (A) and discomfort scores (B). Effect of order (conventional waveform or high-frequency carrier (HFC) waveform first) on PRM reflex threshold (C) and discomfort scores (D). (E) Effect of order (first versus second waveform) on discomfort scores. NS = not significant; error bars represent standard deviation.

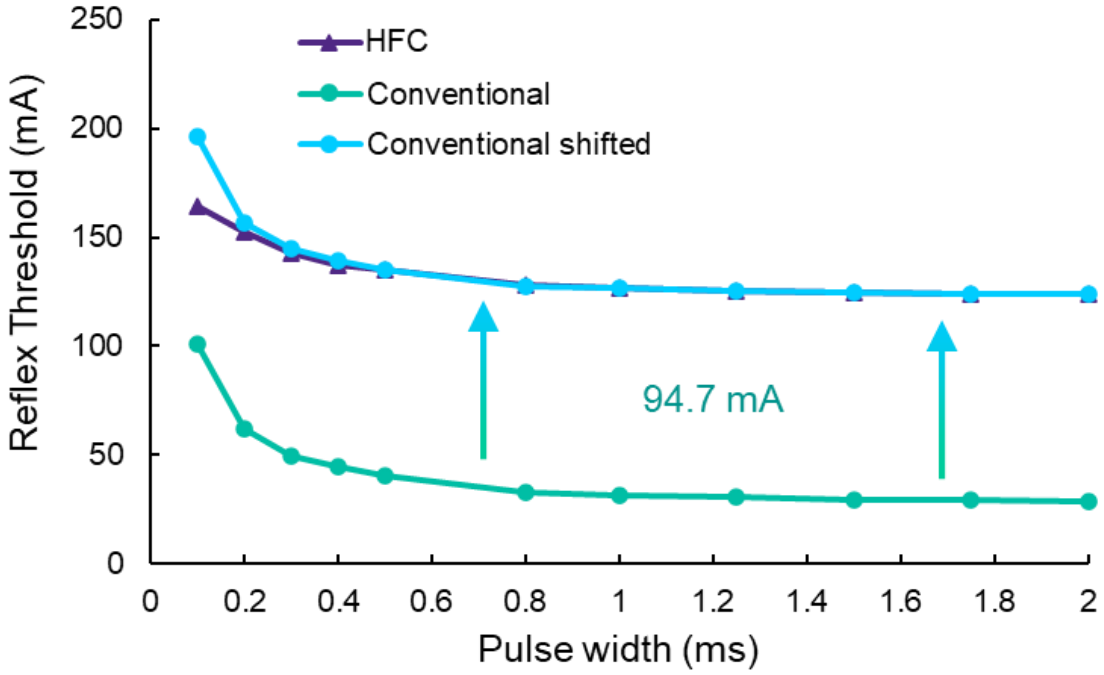

Supplementary Figure 6. Strength-duration curve shift. We shifted the strength-duration curve of the conventional waveform up by 94.7 mA to overlap with the strength-duration curve of the high-frequency carrier (HFC) waveform to demonstrate their likeness. Note: for the HFC waveform, the threshold for pulse durations < 300 μs were > 180 mA; therefore, the curve is incorrectly less steep.